SANDIA REPORT

SAND94–0169 • UC–405
Unlimited Release
Printed August 1994

MICROFICHE

HEISHI: A Fuel Performance Model for Space Nuclear Applications

Michael F. Young

Prepared by
Sandia National Laboratories
Albuquerque, New Mexico 87185 and Livermore, California 94550
for the United States Department of Energy
under Contract DE-AC04-94AL85000

Issued by Sandia National Laboratories, operated for the United States Department of Energy by Sandia Corporation.

Available to DOE and DOE contractors from
Office of Scientific and Technical Information
PO Box 62
Oak Ridge, TN 37831

Prices available from (615) 576-8401, FTS 626-8401

Available to the public from
National Technical Information Service
US Department of Commerce
5285 Port Royal RD
Springfield, VA 22161

NTIS price codes
Printed copy: A04
Microfiche copy: A06

SAND94-0169
Unlimited Release
Printed August 1994

Distribution
Category UC-405

HEISHI: A Fuel Performance Model for Space Nuclear Applications

Michael F. Young
Innovative Nuclear Technology
Sandia National Laboratories
Albuquerque, NM

ABSTRACT

HEISHI is a Fortran computer model designed to aid in analysis, prediction, and optimization of fuel characteristics for use in Space Nuclear Thermal Propulsion (SNTP). Calculational results include fission product release rate, fuel failure fraction, mode of fuel failure, stress-strain state, and fuel material morphology. HEISHI contains models for decay chain calculations of retained and released fission products, based on an input power history and release coefficients. Decay chain parameters such as direct fission yield, decay rates, and branching fractions are obtained from a database. HEISHI also contains models for stress-strain behavior of multilayered fuel particles with creep and differential thermal expansion effects, transient particle temperature profile, grain growth, and fuel particle failure fraction. Grain growth is treated as a function of temperature; the failure fraction depends on the coating tensile strength, which in turn is a function of grain size. The HEISHI code is intended for use in analysis of coated fuel particles for use in particle bed reactors; however, much of the code is geometry-independent and applicable to fuel geometries other than spherical.

ACKNOWLEDGEMENTS

The work described in this report was funded by the Space Nuclear Thermal Propulsion (SNTP) Program. The SNTP program is sponsored by the Air Force and run by the Phillips Laboratory, Kirtland AFB, NM. The author wishes to thank S. A. Wright for many helpful discussions in writing the HEISHI code and this report.

CONTENTS

LIST OF FIGURES

1 INTRODUCTION

1.1 Purpose of HEISHI Model

The purpose of developing the HEISHI Fuel Performance Model is to aid in analysis, prediction, and optimization of fuel characteristics for use in Space Nuclear Thermal Propulsion (SNTP). The information desired is fission product release rate, fuel failure fraction, mode of fuel failure, stress-strain state, fuel material morphology, and chemical behavior of fuel under experimental, operational and accident conditions. The HEISHI code is intended for use in analysis of coated fuel particles for use in particle bed reactors; however, much of the code is geometry-independent and applicable to fuel geometries other than spherical.

1.2 General Description of Features

The current version of HEISHI, Version 2.1, contains models for decay chain calculations for retained and released fission products, based on an input power history and release coefficients. A particle bed temperature profile may also be input to get total release from an entire particle bed. Decay chain parameters such as direct fission yield, decay rates, and branching fractions are obtained from a database.

HEISHI also contains models for stress-strain behavior of multilayered fuel particles with creep and differential thermal expansion effects, a transient particle temperature profile, grain growth, and fuel particle failure fraction. Grain growth is treated as a function of temperature, and the failure fraction depends on the coating tensile strength, which in turn depends on grain size.

Possible areas for future improvement include models for changing particle geometry and morphology to allow treatment of melting and dissolution, and models for coating oxidation and fuel chemistry.

1.3 Intended Application

The intended application of HEISHI is as a tool for evaluating current and proposed fuel designs. Analysis of experimental data on failure and fission product release can be done and related to the stress-strain state in the fuel during the experiment. The same can be done for operational or accident scenarios. A further application is to parametrically investigate designs to attain desired design goals, such as minimizing failure fraction.

The HEISHI code is not limited to a particular fuel particle design or material choice, and can be used to evaluate proposed designs in terms of material selection and number or thickness of layers to attain design goals.

2 FISSION PRODUCT MODELING

2.1 Decay Chain Equations

The equations solved by HEISHI to calculate radionuclide activity are a set of coupled ordinary differential equations representing beta decay chains. There is a set of decay equations for retained nuclides and a coupled set for released nuclides. The decay chain equations are coupled between parent and daughter nuclides in the same chain and between retained and released nuclides. The decay chain equations do not account for other decay modes such as alpha decay.

2.1.1 Simplifying Assumptions

The beta decay equations are solved using some simplifying assumptions:

1. The fission power source is assumed to be uniformly distributed in the first (inner) layer, or core, with no spatial dependence.

2. No decay modes other than beta decay are considered, so that the beta decay chains are uncoupled from one another.

3. The initial inventory of radionuclides is assumed to be zero.

4. Radionuclides are assumed to be either retained in the fuel particle or released. Radionuclide profiles in the coatings or kernels are neglected (Note: an early experimental version of HEISHI does have the capability to calculate transient profiles, but was abandoned because it required detailed knowledge of diffusional release mechanisms which are unknown or not supported by the quality of available experimental measurements).

The decay equations for a single decay chain can be written as

$$\dot{n}_i = \beta y_i - (\lambda_i + \alpha_i) n_i + \sum_j f_{Bji} \lambda_j n_j \qquad (1)$$

and

$$\dot{n}_{Ri} = (\alpha_i - \lambda_i) n_{Ri} + \sum_j f_{Bji} \lambda_j n_{Rj} \qquad (2)$$

where

$\dot{n}_i$ = rate of change in atoms of nuclide i per second,
β = fission source term, fissions per second,
y_i = fractional direct fission yield,

λ_i = decay constant for nuclide i (s^{-1}),
α_i = release coefficient for nuclide i (s^{-1}),
n_j = number of atoms of parent nuclide j,
f_{Bji} = branching fraction for decay of nuclide j to nuclide i,
$\dot{n}_{Ri}$ = rate of change in released atoms of nuclide i per second,
n_{Rj} = number of released atoms of parent nuclide j.

As seen in the above equations, the release coefficient α_i plays the same role in the retained nuclide Eq (1) as the decay constant λ_i and, in the released nuclide Eq (2), the same role as nuclide source. Note that the decay equations are written in terms of total numbers of fission product atoms in the problem. In HEISHI, the input parameters are the reactor power and a coupling factor relating the reactor power to power per unit volume of particle bed; this facilitates use of the code in analyzing reactor experiments. The fission source term β is written in terms of the input parameters as

$$\beta = Q\frac{C_f}{29 \times 10^{-12}}, \qquad (3)$$

where
Q = Input power (W),
C_f = Coupling factor, (W-bed/W-reactor/m^3-bed),

and the factor 29 x 10^{-12} is the Joules per fission.

The product QC_f has the units of bed power in Watts per unit bed volume in m^3. For a self-driven reactor, Q would represent the total reactor power and C_f would represent average power density (W-bed/m^3-bed).

2.2 Release Coefficients

2.2.1 Relation to Release Fraction

The relation of the release coefficients α_i defined above to the release fraction of nuclides can be more easily seen by a simplified example. Neglecting the contribution of the parent nuclide decay, Eq (1) has the solution for a constant fission source β of

$$N_i = \frac{\beta y_i}{\alpha'_i}\left(1 - e^{-\alpha'_i t}\right), \quad \alpha'_i \equiv \alpha_i + \lambda_i \qquad (4)$$

The number of atoms released per second at any time is the product of the number of retained atoms and the release coefficient, so that the fraction f_r of atoms released for nuclide i at any given time can be expressed as the release rate divided by the production rate

$$f_r = \frac{\alpha_i N_i}{\beta y_i} \qquad (5)$$

The total release fraction of nuclide i can be obtained by integrating Eq (5) over the total irradiation time t_Q and dividing by the irradiation time to get

$$F_{ri} = \frac{\alpha_i}{\alpha'_i}\left(1 - \frac{\left(1 - e^{-\alpha'_i t_Q}\right)}{\alpha'_i t_Q}\right) \qquad (6)$$

The release fraction F_{ri} is identical with the release-to-birth ratio (R/B) defined in terms of the direct yield, except that the contribution of parent nuclide decay is neglected.

When the contribution of the parent nuclide is included, the relation is much less clear, since a large part of the R/B ratio can come from parent nuclide decay.

2.2.2 Release Mechanisms – Intact Fuel Particles

The release coefficients should be related to real physical variables if the code is to be used to extrapolate results under conditions very different from the validation data base. Empirically, release coefficients can be determined from experimental release rates, but this procedure does not give any physical insight as to the processes controlling release and does not allow much faith when scaling experimental results to other operating regimes. Release coefficients can also be related to known fission product transport mechanisms such as diffusion through solids.

Diffusion through solids is governed by Fick's Law,

$$J = -D\frac{dc}{dr}, \qquad (7)$$

where

J = atomic flux ($1/m^2$-s),
D = diffusion coefficient (m^2/s),
c = atomic concentration ($1/m^3$),
r = spatial dimension (m).

The diffusion coefficient D is a function of temperature and is usually expressed in the Arhennius form

$$D(T) = D_o e^{-\frac{Q}{RT}} \quad (8)$$

where

D_0 = lead coefficient (m^2/s),
Q = activation energy (J/mol-K),
R = Gas constant (8.314 J/mol-K),
T = temperature (K).

The release rate from a single particle is equal to the atomic flux times the particle area, or JA, where A is the particle area. In terms of Fick's Law, this can be written as

$$JA = AD\frac{dc}{dr} = \alpha n \quad (9)$$

To estimate the release coefficients from (9), the following assumptions are made:

1. The outer coating controls the release rate.

2. The fission product distribution is steady-state in the coating, so that a linear approximation is valid.

3. No storage or holdup of fission products in the coating.

4. Fission product distribution is flat in the interior of the coating.

Given the assumptions for the distribution, Eq (9) can be written as

$$\alpha n = AD\frac{(n/V_c)}{\ell}, \quad (10)$$

where

V_c = volume inside coating (m^3),

from which the release coefficient can be seen to be

$$\alpha = \frac{D}{\ell}\frac{A}{V_c} \quad (11)$$

where

ℓ = thickness of coating (m),
A = area per particle (m^2).

The above formulation assumes that the fission product concentration is spatially uniform in the interior volume of the coating. Another possible assumption is that transport of fission products from the fuel kernel across an internal porous buffer layer (a feature in some particle designs) occurs by gas-phase diffusion rather than solid-phase diffusion. The partial pressure in the buffer layer is then proportional to the fission product mole fraction times the saturation partial pressure in the kernel, so that if a uniform partial pressure in the buffer layer is assumed, the mole fraction at the inner surface of the coating is the same as the mole fraction at the outer surface of the fuel kernel. The effective release coefficient is then given as

$$\alpha n = A \frac{D}{\ell} \chi_c c_c \qquad (12)$$

where

χ_c = mole fraction of fission product at the inner coating surface (in the buffer layer),

c_c = atom concentration of the buffer layer material (m^{-3}).

Since the mole fraction is the same as the kernel mole fraction given by

$$\chi_k = \frac{c}{c_k} = \frac{n}{V_k} \frac{1}{c_k} \qquad (13)$$

where

c_k = atom concentration of the kernel material (m^{-3}),

V_k = the kernel volume (m^3),

the release coefficient can be written as

$$\alpha = A \frac{D}{\ell} \frac{c_c}{V_k c_k} \qquad (14)$$

This method of estimating release coefficients from diffusion coefficients has been found to give good agreement with release activity in gas samples from the Particle Nuclear Test (PNT) experiments for some nuclides thought to be released principally from intact fuel particles. In those experiments, initial release coefficient estimates were derived as above from bulk diffusion coefficients and the resulting calculated releases compared to measured activities from gas samples. Although it is thought that the agreement in this case between calculated and measured release coefficients may be fortuitous, the procedure can also be thought of as a scaling procedure, and used to derive release coefficients from diffusion coefficients for other types of diffusion-governed processes, such as grain-boundary diffusion. The procedure should give reasonably good estimates of the release coefficients in cases where the particles are in a steady-state diffusion mode. An option to calculate release coefficients according to the above formula from bed temperature and the particle material and geometric parameters is included in HEISHI.

2.2.3 Release Mechanisms – Failed Fuel

In the PNT3 and PNT4 experiments, xenon (Xe) was released in larger quantities than seemed consistent with the other nuclides (thought to be released from intact fuel via a diffusional mechanism). Also, in PNT3 the activity increased with consecutive samples, suggesting a continuous release mechanism. The Xe was thought to be released from the surface of failed fuel material. Possible mechanisms for this surface release are release of Xe originally on the grain boundary from the fuel surface, and direct recoil release as the parent nuclide on the surface decays (see Figure 1). This second mechanism suggested a release term of the form

$$\alpha_d n_p = \lambda_p n_p f_{fail} f_d, \qquad f_d = \frac{1}{2}\frac{A_g \delta}{V_g} \qquad (15)$$

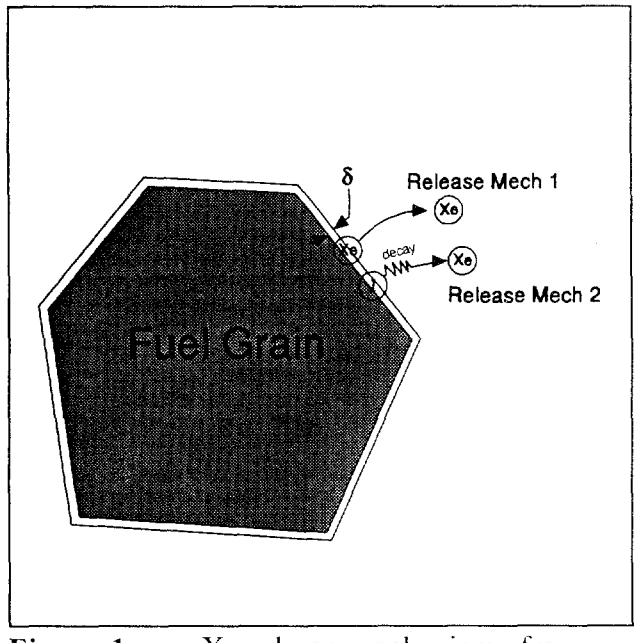

Figure 1 Xe release mechanisms from fuel grain.

where

α_d	=	direct release coefficient (s^{-1}),
f_{fail}	=	fraction of failed fuel,
f_d	=	fraction directly released,
A_g	=	surface area of fuel grain (m^2),
δ	=	effective depth into grain (m),
V_g	=	fuel grain volume (m^3).

In the above derivation, the fraction of the parent nuclide that can directly release the daughter is taken to be 1/2 the amount of parent nuclide atoms within a distance δ of the surface, divided by the grain volume. If the depth δ were interpreted instead as the grain boundary width, then the formula for f_d is seen to be 1/2 the grain boundary volume divided by the grain volume, or 1/2 the fraction of the parent on the grain boundary. The direct release coefficient α_d appears in the retained nuclide decay equation as an additional decay constant in the parent equation, and in the released nuclide equation as an additional release term proportional to the retained parent nuclide.

In the analysis of the PNT3 and PNT4 data, it was observed that the release of Xe from failed fuel appeared to be proportional to the amount of retained Xe, rather than to the retained parent, iodine (I). The dependence on retained Xe was suggested because the parent iodine

decayed too rapidly to match the observed data on Xe activity, even if most of the iodine were released. This observation supports the idea of a direct release mechanism in which the Xe on the grain boundary is released gradually over a period of time, as expressed in Eq (16):

$$\alpha_s n = C_s n f_{fail} \frac{A_g \delta}{V_g} \qquad (16)$$

The actual physical descriptions of these hypothetical direct mechanisms have not yet been resolved. The data from the PNT5A experiment, which included counting of surfaces of experimental components, indicated a release rate of Te-I 300-900 times higher than was apparent from gas sample data, with most of the Te-I adsorbed on the carbon foam insulators. Xe release from these component surfaces via decay of the parents can account for a good portion of the observed gas Xe activity in PNT5A. Presumably, comparable amounts of Te-I were adsorbed on metal surfaces in PNT3 and PNT4, so that the magnitude of Xe release from the surface of failed fuel is uncertain. Surface counts of components in PNT5B also showed comparable Te-I activities. The PNT5B experiment was not fully analyzed due to program cancellation.

2.2.4 Particle Bed Temperature Profile Option

There is an option in HEISHI Version 2.1 to calculate total release from a cylindrical particle bed accounting for a two-dimensional temperature profile in the particle bed. This is done by reading bed geometry and bed temperature information from an input file; the input file is usually generated by a separate code that calculates bed temperature versus radius and height. The temperature distribution is normalized using an input normalization temperature, and the resulting temperature profile shape is assumed to be constant in time. A set of activation energies for the nuclides in the problem are also read from a database. The temperature profile and activation energy are then used to calculate the variation in the read-in release coefficient for each nuclide with bed temperature, and the resulting spatially-dependent release coefficients integrated over the bed volume to give an effective bed release coefficient α for each nuclide, which is used in the decay equations.

Although the above procedure gives a reasonable way to account for bed temperature variations, note that it does not account for a possible spatial profile in reactor power deposition in the bed which may accompany the temperature profile.

3 FISSION PRODUCT CODING AND SOLUTION METHOD

3.1 Finite Difference Equations

The decay chain equations, Eq (1) and Eq (2), form a set of coupled ordinary differential equations (ODEs). To maintain generality in the allowable input form of the power $Q(t)$ and release coefficients $\alpha(T,t)$, the equations are solved by finite difference methods rather than a direct analytic solution.

The decay equations can be expressed in finite difference form as

$$\boldsymbol{n}_k = \boldsymbol{n}_k^n + \boldsymbol{F}(\boldsymbol{n}'_k, t)\,\Delta t, \quad k = 1...NC \tag{17}$$

$$\boldsymbol{n}_{Rk} = \boldsymbol{n}_{Rk}^n + \boldsymbol{F}_R(\boldsymbol{n}'_{Rk}, \boldsymbol{n}'_k, t)\,\Delta t, \quad k = 1...NC \tag{18}$$

where

n_k	=	vector of retained nuclides in decay chain k, each element of the vector being the number of atoms of a nuclide,
$F()$	=	vector of derivatives for the retained nuclides in decay chain k,
n_{Rk}	=	vector of released nuclides in decay chain k, each element of the vector being the number of atoms of a nuclide,
$F_R()$	=	vector of derivatives for the released nuclides in decay chain k,
Δt	=	timestep (s),
NC	=	number of chains.

In the above equations, the derivatives $F()$ and $F_R()$ are shown as functions of time and the other nuclides in the chain. The equation for the nuclide with atomic number Z is only coupled to at most three parent equations: the Z-1 nuclide (direct beta decay), the Z-1M (beta decay from a Z-1 metastable nuclide), and ZM (gamma decay from a Z metastable nuclide). The released nuclide derivatives can also be functions of the retained nuclides if a direct release coefficient is used (release proportional to the retained parent). The time dependence of the derivatives is from the fission source and the release coefficients. The superscript / on the nuclide vectors in the derivatives indicates evaluation at some intermediate time during the timestep, and the superscript n refers to evaluation at the old time.

The derivatives can be written for decay chain k and nuclide i as

$$F_{k,i} = \beta(t)\, y_{k,i} - (\alpha_i(t) + \lambda_{k,i}) n_{k,i}(t) + (1 - \alpha_{di}(t)) \sum_{j=1}^{3} \lambda_j n_{k,j}(t) \qquad (19)$$

$$F_{Rk,i} = \alpha_i(t)\, n_{k,i}(t) - \lambda_{k,i} n_{Rk,i}(t) + \alpha_{di}(t) \sum_{j=1}^{3} \lambda_j n_{k,j}(t) \qquad (20)$$

The surface release coefficient is combined with the diffusion release coefficient $\alpha_i(t)$, since the surface release is also proportional to the retained nuclide.

3.2 Solution Method

The solution method for the set of coupled ODEs described in Eq (17) through Eq (20) is Euler's method, meaning that the derivatives F and F_R are evaluated using old-time values of the nuclide numbers. The actual procedure is a variation of an algorithm (Press 1986, 1992) for solving coupled ODEs, except that the 4th order Runge-Kutta algorithm given there for evaluating the derivatives has been replaced with Euler's method. The Euler solution method has been compared with the Runge-Kutta solution over times of interest for HEISHI applications (minutes to weeks – see **TEST PROBLEMS** Section 4).

The integration procedure is called with a main timestep; the procedure returns the nuclide numbers at the end of the main timestep. Error in the solution is controlled by evaluating the equations over each main timestep twice: at the current integration timestep (which can be smaller than the main timestep) and at half the current integration timestep. If the relative error between the two solutions is greater than an error criterion, the integration timestep is halved and the procedure repeated until convergence is obtained.

3.3 Dropping Insignificant Nuclides

The maximum timestep that can be taken by the ODE integrator is controlled by the shortest halflife nuclide in the problem according to the formula

$$\Delta t_{max} = 0.693 \frac{0.3}{\lambda_{shortest}} \qquad (21)$$

This formula sets the maximum timestep to 0.3 of the shortest half-life. If the maximum timestep could be increased, the number of timesteps taken during the problem could be decreased, and hence the actual computer central processor unit (cpu) time needed for the problem could be decreased. The maximum timestep can be increased by removing short-half-life nuclides from the problem; this is done by noting that the shorter half-life nuclides will, for the most part, decay quickly in the beginning of the problem. As the total number of

retained atoms of a nuclide becomes less than a cutoff limit (10^4 atoms is the current default), the decay equation for the nuclide is dropped from the set of decay equations. The dropping of the short-half-life nuclide is only done when the fission source is zero.

4 TEST PROBLEMS

4.1 Comparison of Euler and Runge-Kutta Methods

In many applications involving integration of ODEs, Euler's method is frowned upon because the method is only second-order accurate in the timestep, thereby usually requiring shorter timesteps than would be required with a more accurate (fourth-order) method to attain a given level of accuracy in the solution. The main benefit of Euler's method is the simplicity of the algorithm and the consequent quick solution times on the computer.

In the present application, the drawbacks of Euler's method are not important for three reasons. The first reason is that the maximum timestep is set by the fastest decaying nuclide in the problem at any moment: the large difference in half-lives between the fastest decaying nuclides, in which we are not interested, and the slower-decaying nuclides, in which we are, ensures that a sufficient number of timesteps will be taken to give good accuracy in the solutions for the slower-decaying nuclides. The second reason is that the release coefficients are generally not known to within more than a factor of 2-5, so inaccuracy in the solution of the ODEs for released nuclides is not particularly important for problems of interest. The third reason is that HEISHI uses an error control algorithm, as described above, to control the error for each timestep. This error control will generally have the effect of producing the same answer with Euler's method as with another more accurate method by using shorter timesteps.

The Euler solution method was compared to a fourth-order Runge-Kutta method (Press and Teukolsky 1992) on a typical HEISHI problem: the solution for the retained and released nuclides in the 133 decay chain for a power history and release coefficients typical of the PNT3 experiment. The problem involved an irradiation of 350 s, during which nuclides were assumed to be released at rates given by the release coefficients, followed by beta decay of the retained and released nuclides. The decay curves were computed to a final time of 10 days.

The comparison revealed that there were differences in the solution on the first timestep of 50% in all nuclides; this is probably a difference in startup characteristics of the algorithms, but involves solutions when the number of atoms of the nuclides are small. The error on the initial timestep had no great effect on the error at later times. A maximum difference of 5% was observed for later times for the fastest decaying nuclide in the chain (I^{133*}, with a half-life of 9 s). Errors for parent nuclides earlier in the chain than I^{133*} were 2-3%; daughter nuclides later in the chain had errors on the order of 1% or less. This level of error is unimportant, given the level of uncertainty in the release coefficients and other experimental parameters.

4.2 Comparison to Analytic Solution

HEISHI calculations for retained nuclides were compared to an analytic solution for a two-nuclide decay chain. The problem was specified as a constant fission source for a given time

t_p, followed by zero power. The initial condition for the two nuclides was zero initial number of atoms, corresponding to the HEISHI assumed initial condition. The two coupled ODEs to be solved are

$$\dot{n}_1 = \beta y_1 - \lambda_1 n_1 , \tag{22}$$

$$\dot{n}_2 = \beta y_2 - \lambda_2 n_2 + \lambda_1 n_1 \tag{23}$$

where the terms are as defined for the HEISHI decay chain equations. The solution is divided into two time intervals: the interval while power is on from 0 to t_p, and the interval while power is off, for $t > t_p$. During the power-on interval, the solution is found for $\beta > 0$ and n_1, $n_2 = 0$ at $t = 0$. For time $t > t_p$, the solution is that for zero source and nonzero initial n_1 and n_2 (given by the power-on solution at $t = t_p$), with the variable t replaced by $t - t_p$.

Table I Parameters for Analytic Comparison

β	y_1	y_2	λ_1	λ_2	t_p
7×10^{12}	0.01	0.01	0.02	0.01	300

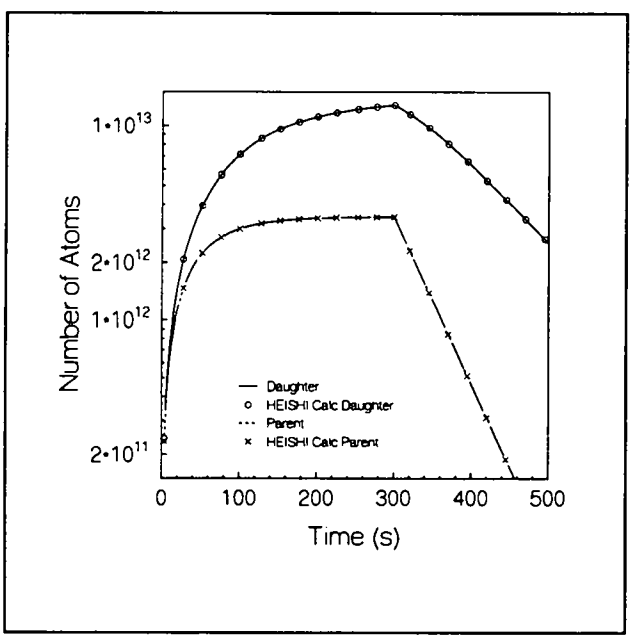

Figure 2 Comparison of analytic solution and calculation for parent-daughter decay

Parameters used for the calculation are given in Table I. These parameters are typical of a fast-decaying nuclide and a typical reactor power-on time for experiments. The decay constant for nuclide 1 is large enough for the solution to approach its limiting value during the irradiation period. Other sets of parameters can be expected to give similar results. The maximum relative error was 1.7% between the analytic result and the HEISHI calculation (Figure 2).

5 STRESS-STRAIN MODELING

5.1 Modeling Assumptions

The HEISHI code contains a stress-strain module adapted from the PSTRESS code (Dobranich 1991). This module solves the stress-strain equations in radial geometry for a multi-layered particle with time-dependent creep and thermal inelastic strains. The time-dependent radial temperature profile in the particle is also solved, including either a volumetric power source in the particle or an applied heat flux on the inner boundary of the (hollow) particle. The stress and temperature results from the stress-strain and temperature solution routines can be input to a grain growth model and failure fraction model.

Although the stress-strain module retains the code structure of the original PSTRESS code, PSTRESS was written to solve the stress-strain and temperature equations in a spherical shell and becomes inaccurate if the inner radius of the shell approaches zero. The stress-strain and temperature equations were therefore written and solved in a different form so that the calculation converges to the correct answers as the inner radius goes to zero, allowing calculation of results for a solid sphere.

The main assumptions of the stress-strain and temperature models are

1. Radial geometry for stress-strain and temperature equations.

2. The stress-strain equations are steady-state. That is, the stress-strain state of the particle is assumed to be instantaneously in equilibrium at any given time, and no transient strain wave solutions are included.

3. Creep rates can be a function of the local shear stress and temperature.

4. Thermal strains are calculated assuming a constant coefficient of thermal expansion for each material layer.

5. The power source is spatially uniform within each material region.

6. Material layers are connected and remain connected – they cannot separate under the influence of tensile stress, and there are no initial internal void regions except possibly in the center.

5.2 Stress-Strain Equations

The stress-strain equations are set up with the inelastic strains treated as extra body forces (Lin 1968). Inelastic strains, as used here, mean any strain which does not obey Hook's law relating stress and strain. The particle is divided into regions, with each region usually corresponding to a separate material layer in the particle. The regions are further divided into

a number of mesh cells in which the material properties, temperature, and inelastic strains can be assumed constant. An equation for the displacement is formed for each mesh cell, with appropriate boundary conditions on the edges of the cells:

1. The innermost cell has an inner BC of either pressure or zero displacement, and an outer BC of continuous displacement.

2. The interior cells have inner and outer BCs of continuous displacement, meaning that the displacement of a cell edge equals the displacement of the adjoining cell edge.

3. The outermost cell has an inner BC of continuous displacement, and an outer BC of specified pressure.

5.2.1 Derivation of Equations

The displacement equation for each cell is derived as in Lin (1968) by substituting the constitutive relations into the equilibrium equation. The constitutive relations can be written as

$$\sigma_r = \lambda(e - e'') + 2\mu(e_r - e_r'') \tag{24}$$

$$\sigma_\theta = \lambda(e - e'') + 2\mu(e_\theta - e_\theta'') \tag{25}$$

where

σ_r = radial stress (Pa),
σ_θ = azimuthal stress (Pa),
λ, μ = Lamé constants
e = total volumetric strain,
e'' = total inelastic strain,
e_r = total radial strain,
e''_r = radial inelastic strain,
e_θ = total azimuthal strain,
e''_θ = azimuthal inelastic strain.

The Lamé constants are written in terms of the material Young's modulus E and Poisson's ratio ν as

$$\lambda = \frac{\nu E}{(1 + \nu)(1 - 2\nu)}, \qquad \mu = \frac{E}{2(1 + \nu)} \tag{26}$$

The compatibility conditions

$$e_r = \frac{du}{dr}, \quad e_\theta = \frac{u}{r}, \quad e = \frac{du}{dr} + 2\frac{u}{r} \tag{27}$$

where

u = radial displacement (m),

r = radial coordinate (m)

are substituted into the constitutive relations to get stress in terms of displacement. The constitutive relations are in turn substituted into the equilibrium equation

$$\frac{d\sigma_r}{dr} + 2\frac{\sigma_r - \sigma_\theta}{r} = 0 \tag{28}$$

to get a differential equation for the displacement

$$(\lambda + 2\mu)\frac{d}{dr}\left[\frac{1}{r^2}\frac{d}{dr}(r^2 u)\right] = \lambda\frac{de''}{dr} + 2\mu\frac{de_r''}{dr} + 4\mu\frac{e_r'' - e_\theta''}{r} \tag{29}$$

This equation can be solved for the displacement by assuming constant material properties λ, μ and integrating twice to get

$$(\lambda + 2\mu)u = \frac{A}{3}r + \frac{B}{r^2} + \frac{1}{r^2}I(r) \tag{30}$$

where A, B are constants to be determined from the boundary conditions, and the term $I(r)$ is defined as

$$I(r) = \lambda\int_a^r r^2 e''dr + 2\mu\int_a^r r^2 e_r''dr + 4\mu\int_a^r r''^2\int_a^{r'}\frac{e_r'' - e_\theta''}{r''}dr''dr \tag{31}$$

where the lower boundary of the cell is at radius a. Given appropriate boundary conditions and expressions for the inelastic strains, the above Eq (30) can be solved for the displacement. Once the displacement is known, the stresses and strains can be readily calculated from the

appropriate equations. The azimuthal and radial strains are, using Eq (30) and the compatibility relations,

$$e_\theta = \frac{1}{\lambda + 2\mu}\left[\frac{A}{3} + \frac{B}{r^3} + \frac{1}{r^3} I(r)\right] \tag{32}$$

and

$$e_r = \frac{1}{\lambda + 2\mu}\left[\frac{A}{3} - 2\frac{B}{r^3} - \frac{2}{r^3} I(r) + \lambda e'' + 2\mu e_r'' + I_1(r)\right] \tag{33}$$

where the integral term $I_1(r)$ is given as

$$I_1(r) = 4\mu \int_a^r \frac{e_r'' - e_\theta''}{r'} dr' \tag{34}$$

The strains can then be plugged into the constitutive relations to get the radial and azimuthal stresses.

5.2.2 Case of Zero Inner Radius

If the inner radius a is zero, then the constant B in Eq (30) is zero. The azimuthal and radial strains are then seen to be equal and constant at $r = 0$ in the absence of inelastic strains. If inelastic strains are present, then both strains have a term involving an integral of the inelastic strains divided by r^3. The limit of this term as $r \rightarrow 0$ must then be evaluated. This will be deferred until the form of the inelastic strains has been determined in the next section.

5.3 Material Constitutive Relations

Material properties needed for the stress-strain solution are E and ν, coefficient of thermal expansion (CTE) α, and a creep law. These properties are needed for each material layer in the problem. Currently, the properties are hardcoded into HEISHI as in the original PSTRESS. Poisson's ratio ν and CTE α are assumed constant and E is a function of temperature. The creep law used can have a variety of forms but must return the creep rate as a function of local principal (Von Mises) stress and temperature.

5.3.1 Thermal Inelastic Strain

The thermal inelastic strains are calculated as

$$e''_{rt} = e''_{\theta t} = \alpha \Delta T, \quad e''_t = e''_{rt} + 2 e''_{\theta t} = 3 \alpha \Delta T, \quad \Delta T = T - T_{ref} \tag{35}$$

where T_{ref} is a reference temperature at which the thermal strains will be zero, for instance the deposition temperature for Chemical Vapor Deposition (CVD) coatings.

5.3.2 Creep Inelastic Strain

The creep law usually is a power law of the form

$$\dot{e}_c = A_c \left(\frac{\sigma}{\beta} \right)^n e^{-\frac{Q}{RT}} \tag{36}$$

where

$\dot{e}_c$	=	creep rate (1/s),
A_c	=	creep constant (1/s),
σ	=	principal (Von Mises) stress (Pa),
β	=	shear modulus (used for normalization) (Pa),
n	=	stress exponent,
Q	=	activation energy for creep (J/mol),
R	=	gas constant = 8.314 J/mol-K,
T	=	temperature (K).

The creep strain for a timestep is calculated from the creep rate as

$$e''_c = \dot{e}_c(\sigma, T) \Delta t + e''^n_c \tag{37}$$

where the stress σ is the Von Mises stress, the superscript n refers to the previous timestep value, and Δt is the stress-strain timestep. The radial and azimuthal components of the creep strain are determined assuming incompressibility, so that

$$e''_{rc} + 2 e''_{\theta c} = 0 \tag{38}$$

and the definition of the Von Mises creep strain (see Dobranich 1991, p. 72-73):

$$e_c'' = s\frac{2}{3}\left(e_{\theta c}'' - e_{rc}''\right) \tag{39}$$

where s is used to give the sign of the creep strain dependent on the order of the principal stresses, so that

$$s = \begin{cases} +1, & \sigma_\theta \geq \sigma_r \\ -1, & \sigma_\theta < \sigma_r \end{cases} \tag{40}$$

The radial and azimuthal creep strains are then given as

$$s e_c'' = 2 e_{\theta c}'' = -e_{rc}'' \tag{41}$$

5.4 Temperature Equations

The radial temperature in the particle is calculated by solving the time-dependent radial heat conduction equation with power source

$$\rho C_p \frac{\partial T}{\partial t} = \frac{1}{r^2}\frac{\partial}{\partial r}\left(k r^2 \frac{\partial T}{\partial r}\right) + q''' \tag{42}$$

where

ρ	=	material density (kg/m^3),
C_p	=	material specific heat capacity (J/kg-K),
k	=	material thermal conductivity (W/m-K),
q'''	=	volumetric power (W/m^3).

The temperature equation can be put in a conservative form suitable for finite difference solution by multiplying the equation by r^2, assuming constant material properties, and formally integrating from $r - \delta r$ to $r + \delta r$ to get

$$r^2 k \left.\frac{\partial T}{\partial r}\right|_{r^+} - r^2 k \left.\frac{\partial T}{\partial r}\right|_{r^-} + \frac{(r^+)^3 - (r^-)^3}{3} q''' = \frac{(r^+)^3 - (r^-)^3}{3} \rho C_p \frac{\partial T}{\partial t} \tag{43}$$

where

$$r^+ \equiv r + \delta r, \quad r^- \equiv r - \delta r. \tag{44}$$

The finite difference equations can then be written by replacing the differential operators by a suitable finite difference form.

6 STRESS-STRAIN CODING AND SOLUTION METHOD

6.1 Finite Difference Equations

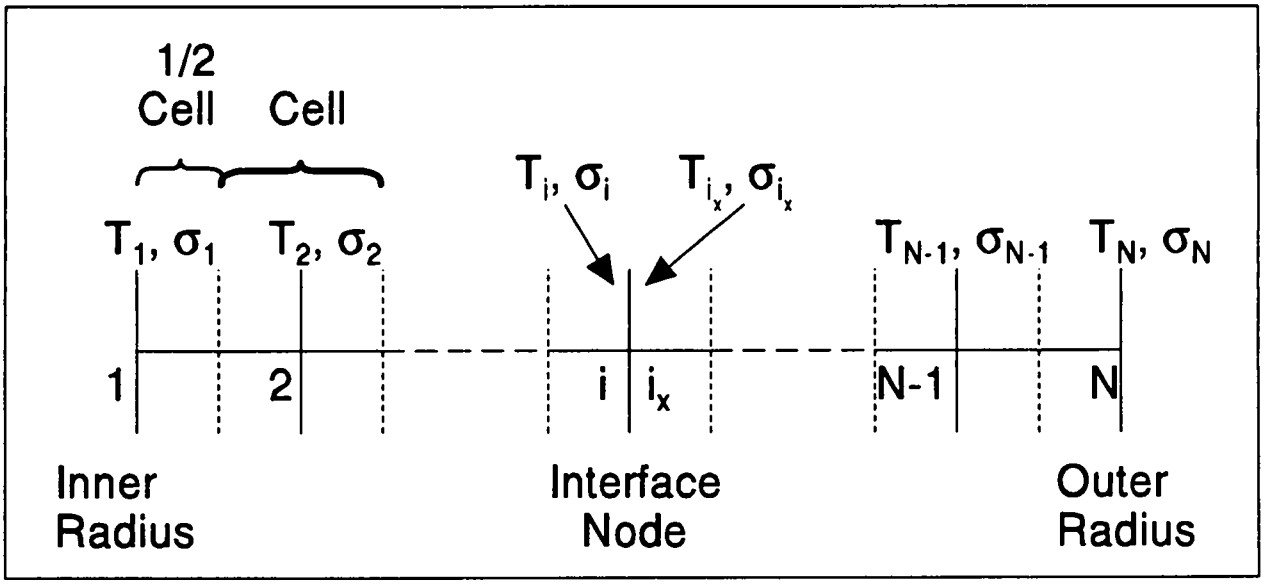

Figure 3 Finite difference mesh for stress-strain and temperature routines.

The finite difference mesh (see Figure 3) is set up with the regions (usually different material layers) divided into a number of grid cells, inside of which properties are assumed constant. Variables such as stress, strain, and displacement are located on the cell edges; this insures continuity of displacement and radial stress. Variables that may be different across an interface where cell edges of two different regions join are handled by including "auxiliary" nodes, as in PSTRESS, at the inner edge of the outer cell of the interface.

6.1.1 Derivation of Finite Difference Equations

The finite difference form of the stress-strain equations are derived by first applying specified displacement boundary conditions to the displacement equation; this results in an equation for u in terms of boundary displacements u_a and u_b:

$$u = (r^3 - a^3)\frac{b^2}{(b^3 - a^3)r^2}u_b + (b^3 - r^3)\frac{a^2}{(b^3 - a^3)r^2}u_a + \frac{1}{(a^3 - b^3)(\lambda + 2\mu)r^2}[(r^3 - a^3)I(b) - (b^3 - a^3)I(r)] \quad (45)$$

This expression for u is then substituted into the constitutive relation for radial stress to get radial stress in terms of the boundary displacements:

$$\sigma_r = \frac{1}{(a^3 - b^3)\, r^2}\{b^2(4a^3\mu + 3r^3\lambda + 2r^3\mu)u_b + a^2(3r^3\lambda + 4b^3\mu + 2r^3\mu)u$$

$$+ \frac{4a^3\mu + r^3(3\lambda + 2\mu)}{(a^3 - b^3)(\lambda + 2\mu)\, r^2} I(b) - 4\frac{\mu}{(\lambda + 2\mu)\, r^2} I(r) + I_1(r) \quad (46)$$

Now, the actual unknowns in the problem are the boundary displacements — the radial stresses are known from the pressure boundary conditions or can be eliminated by subtracting the solutions for two adjoining cells. Substituting known pressure boundary conditions at a and b in the above radial stress equation gives

$$-P_a = \frac{1}{a^3 - b^3}\left\{3I(b) - 3b^2(\lambda + 2\mu)\, u_b + \frac{1}{a}(3\lambda a^3 + 2\mu a^3 + 4\mu b^3)u_a\right\} \quad (47)$$

and

$$-P_b = \frac{1}{a^3 - b^3}\left\{3I(b) - \frac{1}{b}(3\lambda b^3 + 2\mu b^3 + 4\mu a^3)u_b + 3a^2(\lambda + 2\mu)\, u_a\right\} \quad (48)$$
$$+ I_1(b)$$

Define the next cell from b to c. This gives another equation for P_b in terms of the variables in the next cell:

$$-P_b = \frac{1}{b^3 - c^3}\left\{\begin{array}{l} 3I'(c) - 3c^2(\lambda' + 2\mu')\, u_c \\ \qquad + \frac{1}{b}(3\lambda' b^3 + 2\mu' b^3 + 4\mu' c^3)u_b \end{array}\right\} \quad (49)$$

where the superscript $'$ is intended to indicate that the properties could be different in the cell from b to c. Subtracting the two equations for P_b then gives an equation in the unknown boundary displacements u_b and u_c, which are also the displacements on the cell edges (nodes). An equation of this form is used for each interior node in the problem. Interfaces between material layers do not pose any difficulties and are handled the same way, except that some auxiliary node variables are kept for quantities that are different across an interface, such as azimuthal stress, radial strain, and inelastic strains.

The nodes are numbered 1..N starting at the inner radius and going to the outer radius, so that there are N cell edges (nodes) and N-1 cells. Using this numbering convention, the displacement equation for u_i can be written as

$$0 = -\frac{1}{r_i}\left[\frac{\left(3\lambda r_i^3 + 2\mu r_i^3 + 4\mu r_{i-1}^3\right)}{\left(r_i^3 - r_{i-1}^3\right)} + \frac{\left(3\lambda' r_i^3 + 2\mu' r_i^3 + 4\mu' r_{i+1}^3\right)}{\left(r_{i+1}^3 - r_i^3\right)}\right] u_i$$
$$+ 3r_{i+1}^2 \frac{(\lambda' + 2\mu')}{\left(r_{i+1}^3 - r_i^3\right)} u_{i+1} + 3r_{i-1}^2 \frac{(\lambda + 2\mu)}{\left(r_i^3 - r_{i-1}^3\right)} u_{i-1} \qquad (50)$$
$$+ \frac{3}{\left(r_i^3 - r_{i-1}^3\right)} I(r_i) - \frac{3}{\left(r_{i+1}^3 - r_i^3\right)} I'(r_{i+1}) - I_1(r_i)$$

where the convention is used that the unprimed terms are evaluated in cell i, the primed terms are evaluated in cell $i+1$, and the subscript i for quantities defined on cell edges, or nodes (u_i) refers to the left (inner) edge of cell i.

6.1.2 Boundary Conditions

The inner boundary condition can be either a specified pressure condition (if the inner radius is greater than zero, so that the particle is hollow) or a specified zero displacement:

$$\sigma_r(r_1) = -P_{in}, \quad or \quad u(r_1) = 0 \qquad (51)$$

The equation used for an inner pressure BC is

$$-P_{in} = -\frac{1}{r_1}\frac{\left(3\lambda r_1^3 + 2\mu r_1^3 + 4\mu r_2^3\right)}{\left(r_2^3 - r_1^3\right)} u_1 + 3r_2^2 \frac{(\lambda + 2\mu)}{\left(r_2^3 - r_1^3\right)} u_2 \qquad (52)$$
$$- \frac{3}{\left(r_2^3 - r_1^3\right)} I(r_2)$$

The outer boundary condition is always a specified pressure condition:

$$\sigma_r(R_o) = -P_o \qquad (53)$$

The equation used for the outer boundary node is

$$P_{out} = -\frac{1}{r_N}\frac{\left(3\lambda r_N^3 + 2\mu r_N^3 + 4\mu r_{N-1}^3\right)}{\left(r_N^3 - r_{N-1}^3\right)} u_N + 3r_{N-1}^2 \frac{(\lambda + 2\mu)}{\left(r_N^3 - r_{N-1}^3\right)} u_{N-1} \qquad (54)$$
$$+ \frac{3}{\left(r_N^3 - r_{N-1}^3\right)} I(r_N) - I_1(r_N)$$

6.1.3 Treatment of Inelastic Strain Integrals

The inelastic strain integrals are evaluated numerically by using a Simpson's Rule approximation to the integrals over each cell. This was found to give the correct result for the case $r_i = 0$, whereas the trapezoidal rule did not. Simpson's Rule can be expressed as

$$\int_a^b f(x)\,dx \approx \frac{h}{3}(f_0 + 4f_1 + f_2), \quad h = \frac{b-a}{2} \tag{55}$$

where the integration interval is divided into 2 subintervals. When applied to a finite difference cell, the integrand $f(x)$ is generally defined only at the cell edges, so that the midpoint value (f_1 above) must be approximated as some average of the edge values. Using the arithmetic average, the first integral term over the inelastic volumetric strain in Eq (31) is approximated as

$$\begin{aligned} I_a(r_i) &= \lambda \int_{r_{i-1}}^{r_i} r^2 e'' dr \\ &\approx \lambda \frac{r_i - r_{i-1}}{6}\left(r_{i-1}^2 e''_{i-1} + 4\frac{\left(r_{i-1}^2 e''_{i-1} + r_i^2 e''_i\right)}{2} + r_i^2 e''_i \right) \\ &\approx \lambda \frac{\left(r_i^3 - r_{i-1}^3\right)}{3}\frac{\left(e''_{i-1} + e''_i\right)}{2} \end{aligned} \tag{56}$$

The second integral term involving the radial inelastic strain is approximated in a similar manner. The third integral term (the double integral) was numerically integrated as

$$\begin{aligned} I_c(r_i) &= 4\mu \int_{r_{i-1}}^{r_i} r'^2 \int_{r_{i-1}}^{r'} \frac{e''_{r,i} - e''_\theta}{r'} dr' \\ &\approx \frac{4\mu}{6}(r_i - r_{i-1})\frac{(e''_{ri} + e''_{r,i-1}) - (e''_{\theta,i} + e''_{\theta,i-1})}{(r_i + r_{i-1})}\left(r_i^3 - r_{i-1}^3\right) \end{aligned} \tag{57}$$

This form avoids dividing by zero if r_i is zero. The above integral is the result of applying Simpson's rule to the integral of $I_1(r)$ and evaluating $I_1(r)$ as

$$I_1(r_i) = 4\mu \int_{r_{i-1}}^{r_i} \frac{e''_r - e''_\theta}{r}\, dr$$

$$\approx 4\mu(r_i - r_{i-1}) \frac{(e''_{ri} + e''_{r,i-1}) - (e''_{\theta,i} + e''_{\theta,i-1})}{(r_i + r_{i-1})} \qquad (58)$$

Returning to the question of how to handle the integral terms in the equations for the strains when $r_1 \rightarrow 0$, the volumetric inelastic strain contains only a thermal inelastic strain component; the creep inelastic volumetric strain is zero because of the assumption of incompressibility. The thermal strain becomes constant with r as $r \rightarrow 0$, so that the first integral term is of the form

$$I_a(\epsilon) = \lambda \frac{1}{3} \epsilon^3 e'' \qquad (59)$$

where e'' is constant. Since the integral is divided by r^3 in the strain equations, the term in the strain equations

$$\frac{1}{\epsilon^3} I_a(\epsilon) = \lambda \frac{1}{3} e'' = \lambda (\alpha \Delta T) \qquad (60)$$

as ε approaches 0. The thermal strain component of the second term involving e''_r behaves similarly, and the third term and I_1 both have no thermal component.

This leaves the problem of how the terms involving creep strain behave as r_1 goes to zero. The assumption is made that the creep radial strain component in the second integral term becomes constant with r as $r \rightarrow 0$ and can be treated in the same way as the thermal component. The third term can be shown to be zero if the strains are either constant in r or depend on r to some positive power. The I_1 integral can be shown to go to zero if the strains depend on r to a positive power or are identically zero.

6.2 Solution Method

The solution method used is to assemble a set of linear equations for the displacements at the node edges, using Eq (50) for the interior nodes and a different equation for inner and outer boundary nodes. If the inner boundary condition is zero displacement, then u_1 is specified and there are N-1 equations, starting at u_2; if a pressure boundary condition is used at the inner boundary, then there will be N equations. The equation for u_N is Eq (54) and, if an inner pressure boundary is specified, Eq (52) is used for u_1. The boundary pressures and inelastic integrals (evaluated using old timestep values) form a source vector; the coefficients

of the displacements form a tri-diagonal matrix; the system of linear equations can then be solved using the Thomas algorithm.

After solving for the displacements, the stresses and total strains are obtained from the appropriate equations. The stresses are then used to calculate new creep strains, which are compared with the old timestep strains; if there is more difference in the strains than an input convergence criterion, then the displacement equations are iterated using the new creep strains. This is the same procedure as in PSTRESS, but in HEISHI the usual result if iteration occurs is to not converge; therefore, it is advisable, if creep strains are not converging, to reduce the stress-strain timestep rather than to iterate.

7 QUALITY ASSURANCE TESTING FOR THE STRESS-STRAIN MODULE

Acceptance testing for the HEISHI stress-strain module consisted of two parts: comparison of results from HEISHI calculations of stress-strain problems to analytic solutions of the same problems, and comparison of results calculated using the HEISHI algorithm in Mathcad to the analytic solution. Comparisons were done of stress, displacement, total strain, and inelastic strain at boundaries and internal interfaces (if any). The problems used for testing are described below. The material properties for all cases were E = 20.7 GPa and ν = 0.3 (λ = 11.94 GPa and μ = 7.96 GPa) and the geometry is shown in Figure 4. In all tests on hollow spheres, the inner radius a = 0.1 cm; the outer radius b is always 0.25 cm.

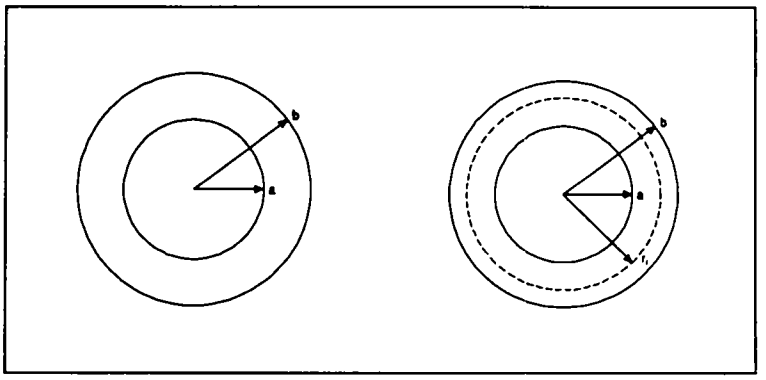

Figure 4 Geometries used for stress-strain tests.

7.1 ST1 – Hollow Sphere with Internal Pressure

In this test, the analytic solution for stress and strain in a hollow sphere with constant material properties was used (Lin 1968, p. 242):

$$\sigma_r = \frac{1}{b^3 - a^3}\left[-(b^3 P_o - a^3 P_i) + a^3 b^3 (P_o - P_i)\frac{1}{r^3}\right] \qquad (61)$$

$$u = \frac{1}{b^3 - a^3}\left[-\frac{r}{\lambda + 2\mu}(b^3 P_o - a^3 P_i) - \frac{1}{4\mu}\frac{a^3 b^3}{r^2}(P_o - P_i)\right] \qquad (62)$$

Inner and outer pressure boundary conditions for ST1 were P_i = 10 MPa and P_o = 0.

The same problem was set up for HEISHI using 20 finite difference nodes and the solutions compared. The standard deviation in the radial stress solution was 0.0009 MPa and that in the displacement was 1.4 x 10^{-7} cm, which should be compared to the maximum radial stress of -10 MPa and the maximum displacement of 3.5 x 10^{-5} cm at $r = a$. The radial stress and displacement results for the analytic solution and the calculation are shown in Figure 5.

7.2 ST2 – Hollow Sphere with External Pressure

This test is the same as ST1 except that the outer pressure P_o is 10 MPa and the inner pressure P_i is 0. The same standard deviations between the calculation and the analytic solution were obtained as in ST1. The maximum radial stress is -10 MPa and the maximum displacement is -5.7 x 10^{-5} cm at $r = b$. The results are shown in Figure 6.

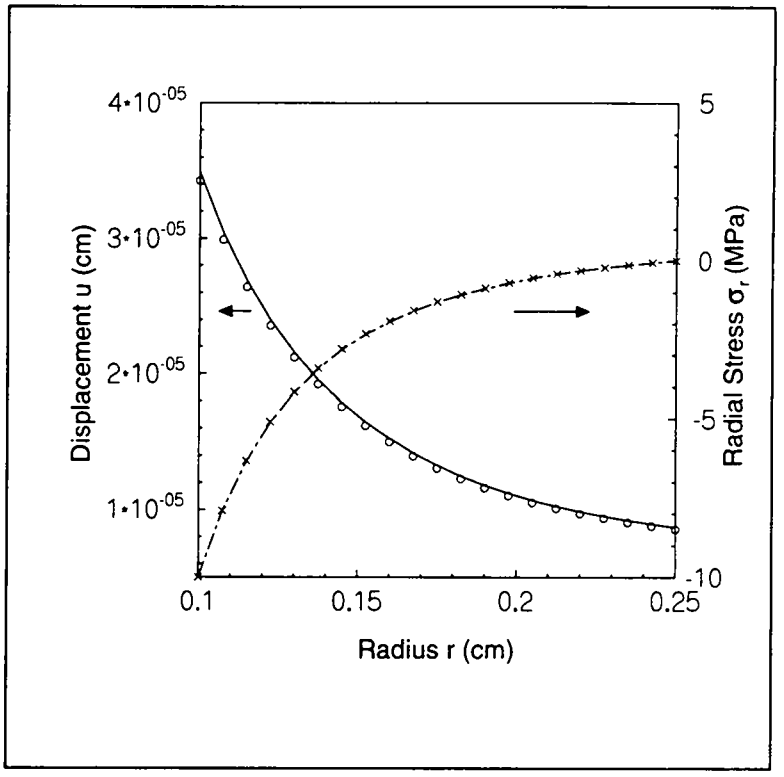

Figure 5 ST1 radial stress and displacement.

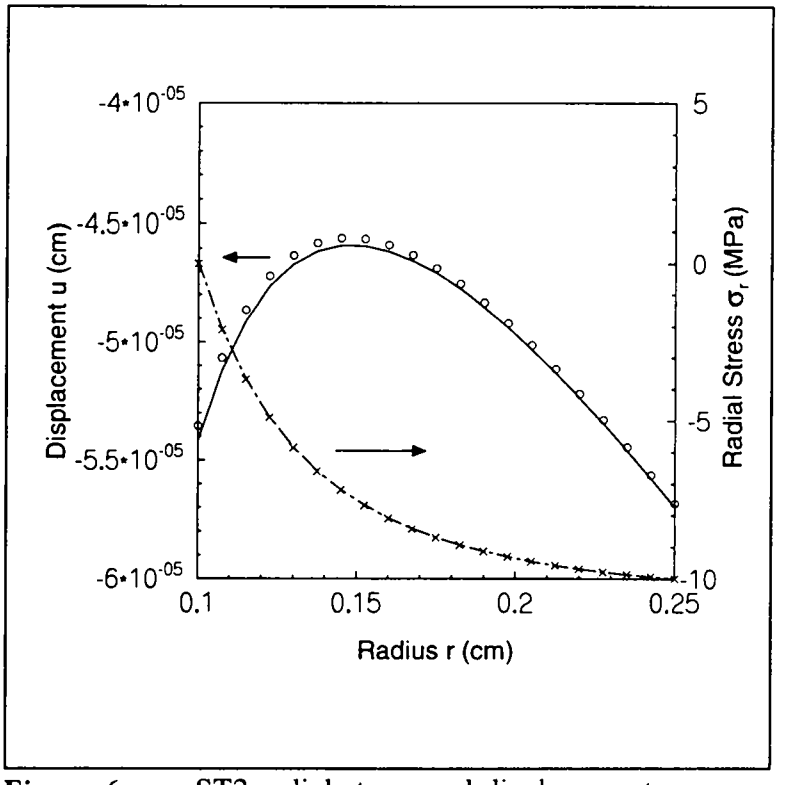

Figure 6 ST2 radial stress and displacement.

7.3 ST3 – Hollow Sphere with External Pressure and Zero Displacement Inner Boundary

This test is the same as ST2, except that the inner pressure boundary condition is replaced by an inner zero displacement boundary condition. The equations for radial stress and displacement for these boundary conditions are different than for inner and outer pressure boundary conditions:

$$\sigma_r = -P_o b^3 \frac{1}{(3\lambda + 2\mu) b^3 + 4\mu a^3} \left[(3\lambda + 2\mu) + 4\mu \frac{a^3}{r^3} \right] \tag{63}$$

$$u = -P_o b^3 \frac{r}{(3\lambda + 2\mu) b^3 + 4\mu a^3} \left[1 - \frac{a^3}{r^3} \right] \tag{64}$$

The comparison between the calculation and the analytic solution was again very good (see Figure 7). The radial stress in this problem starts at -10 MPa at the outer boundary and decreases to -15.5 MPa at the inner boundary, while the magnitude of the displacement is maximum on the outer boundary (-4.2 x 10^{-5} cm) and decreases to zero at the inner boundary. Note that taking the limit of the above equations as $a \rightarrow 0$ to derive the equations for a solid sphere only works for the displacement - the radial stress equation always has an extra term, which produces an increase in the calculated radial stress near $r = 0$. The actual radial stress is a constant with r for this problem. I mention this because instructions for finite element stress-strain computer codes, and even some "stress-strain cookbooks", sometimes recommend letting the inner

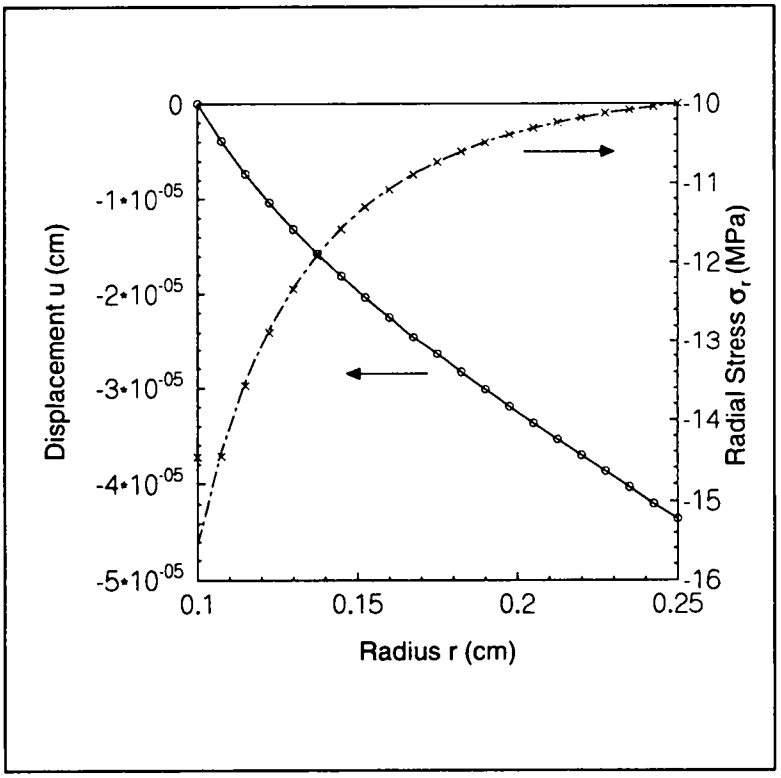

Figure 7 ST3 radial stress and displacement comparison.

radius approach zero as a way to get the answer to a solid sphere problem, which will not work.

An example of the solution obtained with the hollow sphere equations by letting $a \rightarrow 0$ is shown in Figure 8. As can be seen by comparing the solution in Figure 8 to the equations for a solid sphere in the next section (ST4), the hollow-sphere solution approaches the real solution except near $r = 0$, where there is a slight deviation in the displacement solution and a large deviation in the radial stress. Curiously, the deviation in the radial stress approaches a constant as $a \rightarrow 0$, but remains in the radial stress solution, whereas the displacement approaches 0 (the correct solution at $r = 0$).

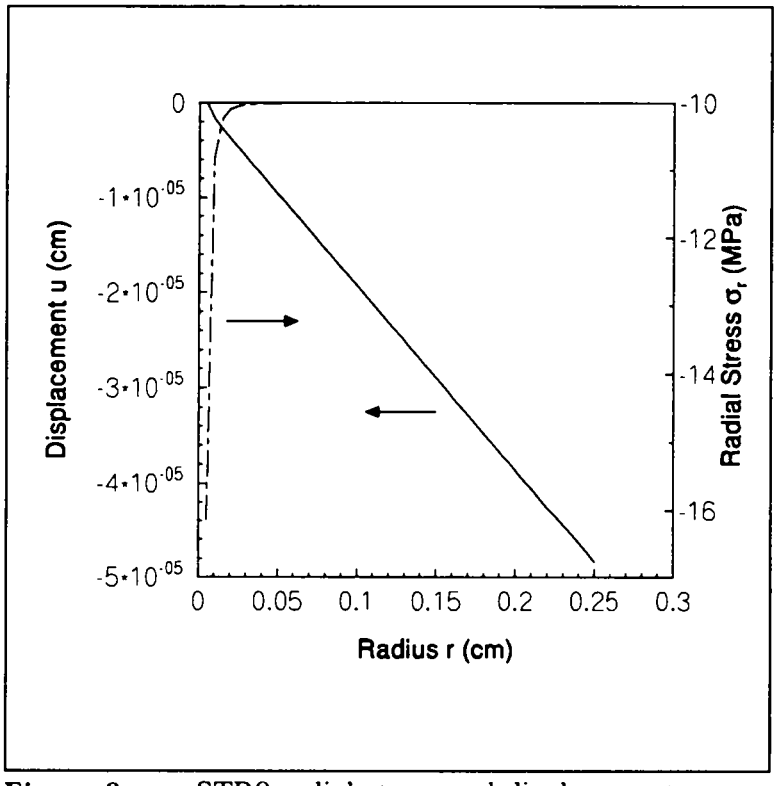

Figure 8 STR0 radial stress and displacement solutions as a $\rightarrow$ 0.

7.4 ST4 – Solid Sphere with External Pressure

This test is the same as ST3 except that the inner radius is zero and the sphere is solid. The equations for the solid sphere under external pressure are

$$\sigma_r = -P_o \qquad (65)$$

$$u = -P_o \frac{r}{3\lambda + 2\mu} \qquad (66)$$

As can be seen from the equations, the radial stress is a constant equal to -10 MPa and the displacement has maximum magnitude at the outer boundary (-4.8 x 10^{-5} cm), decreasing linearly to zero at $r = 0$. The comparison was again very good.

7.5 ST5 – Hollow Sphere with Thermal Inelastic Strain

For this test, inner and outer pressure boundaries were both set to zero and an analytic solution (Pilkey and Chang 1978, p.267) was used for the comparison: the result for constant thermal strain is, of course,

$$\sigma_r = 0 , \quad u = r\alpha (T - T_{ref}) \qquad (67)$$

where the displacement corresponds to the result for constant thermal strain (see Eq (35)). A CTE of α = 12 x 10^{-6} and ΔT of -1350 K were used, giving a maximum displacement of -0.0041 cm. Again, no significant error was seen in the comparison results.

7.6 ST6 – Solid Sphere with Thermal Inelastic Strain

The analytic solution was again from Pilkey and Chang (1978), but with a = 0; the equations and results are the same as for ST5.

7.7 ST7 - Interference Pressure in Two-Region Hollow Sphere

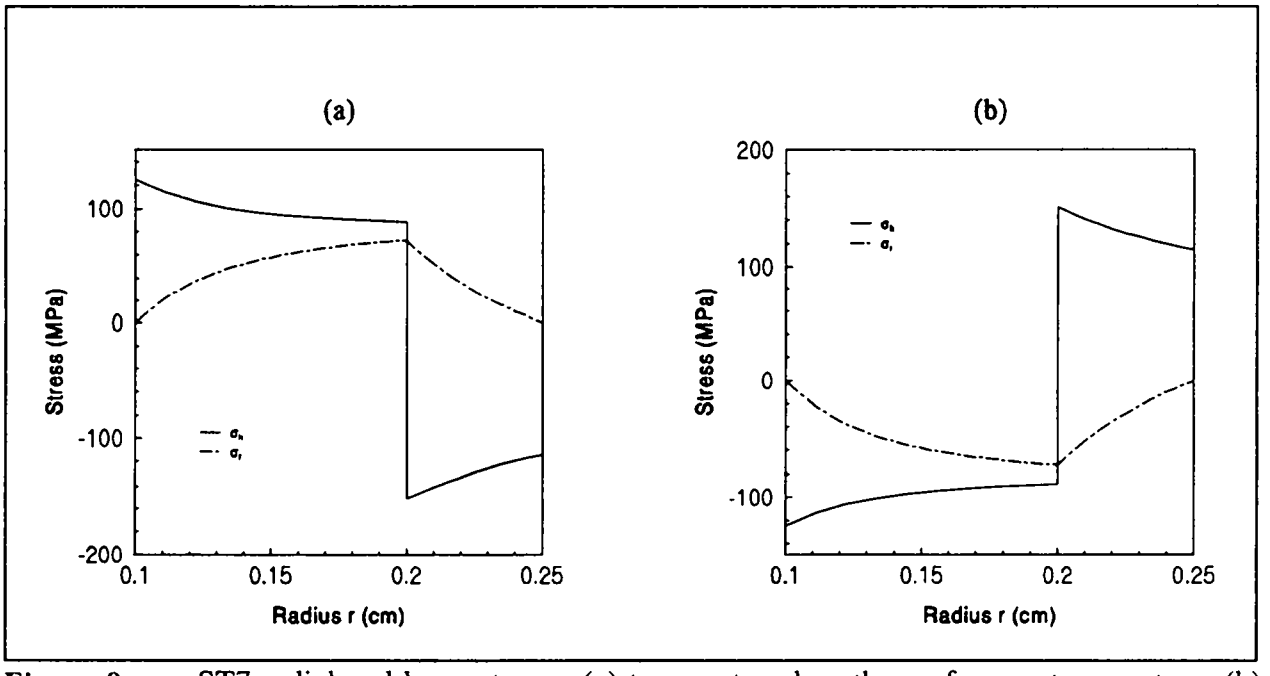

Figure 9 ST7 radial and hoop stress: (a) temperature less than reference temperature; (b) temperature higher than reference temperature.

This problem was intended to test the calculation of interference pressures between two regions with unequal CTEs. A constant temperature was assumed across a hollow spherical shell consisting of two regions with the inner region having a higher CTE than the outer region. The CTE for the inner region was the same as in ST5 and ST6, and the CTE for the

outer region was assumed to be 6 x 10^{-6}. Material properties were otherwise the same in both regions (same as in previous tests). The geometry was also the same as for the previous tests, except that there was a region boundary at r = 0.2 cm. Cases were tried for temperatures both higher and lower than the reference temperature, resulting in both compressive and tensile interference pressures. In case (a), the temperature was 1350 K lower; in case (b), the temperature was 1350 K higher. The analytic solution is Eq 4.5-2 and Eq 4.5-3 from Dobranich (1991) (note that the definition of the $\alpha\Delta T$ terms in 4.5-3 results in division by a factor of 3 for a constant ΔT, versus the definition given in Eq (35)). No significant error was seen in the comparison. The radial and hoop stress for both cases are shown in Figure 9.

8 RADIAL TEMPERATURE EQUATIONS AND SOLUTION METHOD

8.1 Finite Difference Equations

The finite difference equations for the radial temperature solution are set up on the same mesh grid as the stress-strain equations (see Figure 3). There are again N nodes, and a convective boundary condition is used on the outer boundary. The inner boundary condition can be either the radial gradient equal to 0 or a specified heat flux.

The equations are set up as a set of linear equations, with the coefficients of the unknown temperatures forming a tri-diagonal matrix and the boundary terms and power source forming a source vector. The general form of the equation is derived from Eq (43) by replacing the derivatives with finite differences and assuming constant node spacing, thermal conductivity evaluated at the average temperature of the two adjoining nodes, as

$$(r_i^+)^2 k_i \left(\frac{\overline{T}_{i+1} - \overline{T}_i}{\Delta r} \right) - (r_i^-)^2 k_{i-1} \left(\frac{\overline{T}_i - \overline{T}_{i-1}}{\Delta r} \right) + V_i \overline{q}_i = V_i (\rho C_p)_i \frac{T_i - T_i^n}{\Delta t} \quad (68)$$

where subscript i refers to the i^{th} node, Δt is the timestep, superscript n refers to the old temperature, and the bar refers to the degree of implicitness:

$$\Delta r = 2\delta r, \quad V_i = \frac{1}{3}\left((r_i^+)^3 - (r_i^-)^3 \right), \quad \overline{T} = \gamma T + (1-\gamma) T^n \quad (69)$$

In terms of the mesh grid, the nodes refer to the cell edges and the radii r_i^+ and r_i^- are cell-centered. When $\gamma = 0$, the equation is explicit; when $\gamma = 1$, the equation is implicit; and when $\gamma = 0.5$, the equation is time-centered (Crank-Nicholson form). There is one equation for each node, forming a set of simultaneous equations. Since each equation is coupled only to its neighbors, the resulting coefficient matrix is tridiagonal and the solution can be found easily using the Thomas algorithm. The equation for the i^{th} node is of the form

$$a_i T_{i-1} + b_i T_i + c_i T_{i+1} = d_i \quad (70)$$

where the coefficients are, for the general case,

$$a_i = (r_i^+)^2 k_i \frac{1}{\Delta r} \gamma, \quad c_i = (r_i^-)^2 k_{i-1} \frac{1}{\Delta r} \gamma, \quad (71)$$

$$b_i = -\left((r_i^+)^2 k_i \frac{1}{\Delta r} + (r_i^-)^2 k_{i-1} \frac{1}{\Delta r} \right) \gamma - V_i \frac{(\rho C_p)_i}{\Delta t}, \quad (72)$$

and

$$
\begin{aligned}
d_i = & -\left((r_i^+)^2 k_i \frac{1}{\Delta r} T_{i+1}^n + (r_i^-)^2 k_{i-1} \frac{1}{\Delta r} T_{i-1}^n \right) (1-\gamma) \\
& -\left(-(r_i^+)^2 k_i \frac{1}{\Delta r} - (r_i^-)^2 k_{i-1} \frac{1}{\Delta r} \right) T_i^n (1-\gamma) \\
& - (\rho C_p)_i V_i \frac{T_i^n}{\Delta t} - V_i (q_i(t)\,\gamma + q_i(t^n)\,(1-\gamma))
\end{aligned}
\tag{73}
$$

These general coefficients must be modified at the inner and outer boundaries of the problem and at interfaces between layers.

8.2 Boundary Conditions

At the inner radius (node $i = 1$), either an adiabatic condition or a specified heat flux boundary can be used. These are both applied the same way, with the adiabatic condition having a heat flux of zero. The boundary condition is expressed analytically as

$$
q'' = -k \frac{\partial T}{\partial r} \tag{74}
$$

and, referring back to Eq (43), the heat flux at the inner boundary (second term) is replaced by the specified external heat flux. This affects terms in the a_l, b_l, and d_l coefficients. Also, since the temperature for node 1 is on the inner radius, the inner node boundary r_l^- is equal to the inner radius r_l. The modified coefficients are

$$
a_1 = 0, \quad b_1 = -(r_1^+)^2 k_1 \frac{1}{\Delta r} \gamma - V_1 \frac{(\rho C_p)_1}{\Delta t}, \tag{75}
$$

and

$$
\begin{aligned}
d_1 = & -(r_1^+)^2 k_1 \frac{1}{\Delta r} T_2^n (1-\gamma) + (r_1^+)^2 k_1 \frac{1}{\Delta r} T_1^n (1-\gamma) \\
& - (\rho C_p)_1 V_1 \frac{T_1^n}{\Delta t} - V_1 (q_1(t)\,\gamma + q_1(t^n)\,(1-\gamma)) \\
& - (r_1^-)^2 (q''(t)\,\gamma + q''(t^n)\,(1-\gamma))
\end{aligned}
\tag{76}
$$

where $q''(t)$ is the time-dependent specified heat flux. For an adiabatic boundary, the q'' in the equation for d_l is set to 0.

The outer boundary condition is specified by setting the heat flux at the outer radius equal to a convective boundary condition, expressed analytically as

$$h\,(T - T_{cool}) \;=\; -k\,\frac{\partial T}{\partial r} \tag{77}$$

This affects the b, c, and d coefficients for the outer node N. The temperature at node N is also on the outer radius, so the outer node boundary r_N^+ is equal to the outer radius r_N. The modified coefficients are

$$c_N = 0\,, \quad b_N = -\left((r_N^+)^2 h(t) \;+\; (r_N^-)^2 k_{N-1}\,\frac{1}{\Delta r} \right)\gamma \;-\; V_N \frac{(\rho\, C_p)_N}{\Delta t}\,, \tag{78}$$

and

$$\begin{aligned} d_N = &-(r_N^-)^2 k_{N-1}\,\frac{1}{\Delta r}\,T_{N-1}^n\,(1-\gamma) \;-\left[-(r_N^+)^2 h(t) \;-\; (r_N^-)^2 k_{N-1}\,\frac{1}{\Delta r} \right] T_N^n\,(1-\gamma) \\ &-(\rho C_p)_N V_N \frac{T_N^n}{\Delta t} \;-\; V_N\left[q_N(t)\,\gamma \;+\; q_N(t^n)\,(1-\gamma) \right] \\ &-(r_N^+)^2\left[h(t)\,T_{cool}(t)\,\gamma \;+\; h(t^n)\,T_{cool}(t^n)\,(1-\gamma) \right] \end{aligned} \tag{79}$$

where the convective heat transfer coefficient $h(t)$ and coolant temperature $T_{cool}(t)$ are both functions of time.

8.3 Interface Conditions

At an interface between layers, the temperature node lies on the interface. The interface node thus includes regions from the two layers forming the interface. Since the layers can have different material properties and different node widths, the energy storage term (RHS of Eq (68)) is modified to use the volume average of the heat capacity. The volumetric heat source is also modified to be the volume average. These changes affect the b and d coefficients for the interface node, with the understanding that the Δr in the two flux terms in Eq (68) is the distance between the two temperatures in the numerators.

In the actual coding, it is useful to keep the concept of auxiliary nodes at an interface, even though there is actually only one temperature (and one linear equation) at an interface. The auxiliary node variables provide storage for extra terms needed at the interface, which are a ρC_p term evaluated at the interface temperature using properties of the next adjoining layer, and volume and heat source terms for the next adjoining layer. If the auxiliary terms for

interface node i are denoted by the additional subscript x, then the energy storage term for the b_i coefficient is written as

$$-(V_i (\rho C_p)_i + V_{ix} (\rho C_p)_{ix}) \frac{1}{\Delta t} \tag{80}$$

where the volumes are

$$V_i = \frac{1}{3}\left(r_i^3 - (r_i^-)^3\right), \quad V_{ix} = \frac{1}{3}\left((r_i^+)^3 - r_i^3\right) \tag{81}$$

A corresponding term appears in the d_i coefficient. The heat source term is similarly rewritten as

$$V_i\left(q_i(t)\,\gamma + q_i(t^n)\,(1-\gamma)\right) + V_{ix}\left(q_{ix}(t)\,\gamma + q_{ix}(t^n)\,(1-\gamma)\right) \tag{82}$$

9 QUALITY ASSURANCE TESTING FOR TEMPERATURE ALGORITHM

Acceptance testing for the HEISHI temperature algorithm was done by comparing the results of a calculation by HEISHI to an analytic solution. The test problem was in spherical geometry and had internal heat generation in a central core, a non-heat generating outer shell, and a specified outer convective boundary condition. The problem was allowed to run until steady-state was achieved (defined as when the internal power generation in equals the convective heat flux out) and the resulting centerline and surface temperatures compared to the analytic result. Agreement was very good, and no error was observed between the analytic result (done with Mathcad) and the HEISHI finite difference solution.

10 GRAIN GROWTH AND FAILURE FRACTION MODELS

Grain growth can occur in ceramics and metals as the temperature is increased. The increased grain size can then have an effect on the ultimate tensile stress of the material. A simple model is included in HEISHI to describe grain growth in the particle layers. A simple failure fraction model based on brittle fracture theory and a Weibull failure distribution (Weibull 1951) is also included, which uses the grain size as a parameter.

10.1 Grain Growth Model

The grain growth model assumes that grain growth can be described by a parabolic rate law with an Arrhenius temperature dependence for the rate (Burke and Turnbull 1952):

$$a^2 = a_o^2 + K_o t e^{-\frac{Q_g}{RT}} \qquad (83)$$

where

a = average grain size (m),
a_o = initial average grain size (m),
K_o = rate constant (m^2),
Q_g = empirical activation energy for grain growth (J/Mol-K).

This equation approximately describes normal grain growth kinetics in a variety of ceramics and metals (Simpson et al. 1971). As used in HEISHI, the above equation is used to describe the grain growth in each material region, or layer, using an average temperature in the layer.

10.2 Failure Fraction Model

The failure fraction model assumes that failure fraction of the particles, with failure defined here as the brittle failure of the outer coating layer, can be described by a Weibull distribution (Weibull 1951). The Weibull distribution is based on the idea that failure is controlled by the "weakest link", in this case the largest flaw in the material. This type of behavior is typical of brittle failure in ceramic materials. The assumption is also made that failures in ceramic particles occur due to brittle fracture, an assumption that is true at temperatures up to the brittle-to-ductile transition temperature of the material. The Weibull distribution is used in the form (Evans et al. 1972)

$$f = \left(1 - e^{-\left(\frac{\sigma_t}{\sigma_o}\right)^m}\right) \qquad (84)$$

where

f = fraction of particles in sample population that fail,
σ_t = effective tensile stress (Pa),

σ_o = normalization parameter for sample population distribution, here taken equal to the fracture stress (Pa),

m = Weibull modulus (5-20).

The Weibull modulus reflects the degree of variability of the fracture strength in the sample population, with higher values indicating less variability. The range 5-20 is typical of ceramics (Davidge 1979, p. 136), and a value of m = 6 is the default in HEISHI (Evans et al., 1972, gave a value of m = 8 for SiC coated particles). The Weibull distribution can be used to relate failure probabilities in different volumes of material by including the volume V in the exponent, but as used here to relate failure probabilities of the same particle design under different stress conditions, the volume term is not necessary. The variation of the maximum tensile stress through the thickness of the outer layer is accounted for by calculating the effective tensile stress as

$$\sigma_t = \frac{1}{V}\int \sigma_{tmax} dV, \quad \sigma_{tmax} = \max(0, \sigma_r, \sigma_\theta) \tag{85}$$

where the integral is over the volume of the outer layer, and the integrand is the maximum tensile stress, taken as the maximum positive principal stress.

To relate grain size to fracture stress, use is made of the fact that the fracture stress is inversely proportional to a critical crack size (Griffith 1920, 1924):

$$\sigma_f \propto \frac{1}{\sqrt{C}} \tag{86}$$

Under the assumption that the failure is controlled by the weakest link (Weibull 1951), failure is controlled by the largest crack (flaw) size, which gives the lowest fracture stress. Further assuming that this critical crack size is proportional to the grain size (Davidge 1979) gives the needed relation between the grain size and the fracture stress:

$$\sigma_f = \sigma_{fo}\sqrt{\frac{a_o}{a}} \tag{87}$$

where σ_{fo} is the fracture stress for the initial grain size in the as-fabricated particle. No temperature dependence is included in the fracture stress (other than indirectly through the grain size) because fracture stress in ceramics is essentially temperature-independent until the temperature exceeds the brittle-to-ductile transition temperature, which is about 0.6-0.7 of the melting temperature for ceramics.

11 CODE STRUCTURE

The overall code structure consists of input and initialization routines, followed by a main loop wherein the runtime routines are called once every main timestep. The stress-strain routines are on a sub-timestep, so that a main stress-strain controlling routine is called with the main timestep, and the control routine then calls the stress-strain solution routines using the stress-strain sub-timestep until the main timestep is covered. The main timestep is increased according to a user-input criterion, limited to a fraction of the halflife of the fastest decaying nuclide present at any given time at the rate determined by the input factor.

Output occurs at plot time intervals which are separately defined for the decay chain and stress-strain output files. Output intervals for the decay chains are increased based on a user-input criterion, while the stress-strain output occurs at a fixed user-input time interval. Output can be forced at a specific time by including either a real or dummy time-power pair in the power-time history input table. Forcing output in this manner will reset the output interval, which will then start to increase again.

12 SUMMARY

This report describes the equations, calculational procedures, and features of HEISHI Version 2.1. HEISHI is currently capable of analyzing fission product release data for a large variety of particle bed problems, and of calculating and predicting the stress-strain behavior of a large class of multilayer particle designs.

As mentioned before, HEISHI does not account for spatial variation in fission product generation rates within a bed, and the time-dependent release coefficients are read-in empirical values, although there is some provision to calculate initial estimates from diffusion coefficients. The HEISHI stress-strain module also does not account for geometry changes during a problem such as separation of layers due to internal tensile stress, or melting of one or more of the layers. The modeling of these effects and inclusion of their effect on release rates is an area for future improvements in the code.

13 REFERENCES

Burke, J. E. and Turnbull, D. (1952), Prog. Metal Phys. III, Pergamon Press, p. 220.

Davidge, R. W. (1979), Mechanical Behaviour of Ceramics, Cambridge Solid State Science Series, Cambridge University Press.

Dobranich, D. (1991), "Heat Transfer and Thermal Stress Analyses of the Multilayered Spherical Fuel Particles of a Particle Bed Space Nuclear Reactor," SAND90-1032, Sandia National Laboratories, Albuquerque, NM.

Evans, A. G., Padgett, C., and Davidge, R. W. (1972), "Strength of Pyrolytic SiC Coatings of Fuel Particles for High-Temperature Gas-Cooled Reactors," *J. Am. Cer. Soc.*, **56** (1), p. 36.

Griffith, A. A. (1920), "The Phenomena of Rupture and Flow in Solids," *Philos. Trans. R. Soc. London* **A221**, p. 163.

Griffith, A. A. (1924), "The Theory of Rupture," *Proc. First Intl. Congress on Applied Mech.*, Delft.

Lin, T. H. (1968), Theory of Inelastic Structures, John Wiley & Sons, Inc.

Pilkey, W. D. and Chang, P. Y. (1978), Modern Formulas for Statics and Dynamics, McGraw-Hill.

Press, W. H. et al. (1986), Numerical Recipes, Cambridge University Press, p. 550.

Press, W. H. and Teukolsky, S. A. (1992), "Adaptive Stepsize Runge-Kutta Integration," *Computers in Phys.*, **6** (2), p.188.

Simpson, C. J. et al. (1971), "The Four Stages of Grain Growth," *Met. Trans.*, **2**, p. 993.

Weibull, W. (1951) "A Statistical Distribution Function of Wide Applicability," *J. Appl. Mech.*, **18**, p. 293.

14 APPENDIX - HEISHI INPUT/OUTPUT MANUAL

This appendix describes the input and output for the HEISHI V2.1 fuel particle code. Version 2.1 contains a solver for decay chains of retained and released fission products, a stress-strain module with creep strains, and models for grain growth and failure fraction. The stress-strain module is derived from PSTRESS. The grain growth model uses input parameters and a parabolic rate equation to describe grain size as a function of time and temperature. The failure fraction model assumes a Weibull distribution with an inputWeibull modulus and initial mean failure stress. The mean failure stress can vary with the grain size. All input is read in from the main input file **hs2.in** described below.

hs2.in format

The input is free format and generally consists of a descriptive line followed by the corresponding input. In some cases, such as tables and decay chains, the descriptive line will contain a variable followed by a slash (/); this means that the variable before the slash is on a line by itself and the variables following the slash are on the next line -- possibly repeated.

I. TITLE1 (A)
This is an alphameric field describing the problem input

II. TITLE2 (A)
This is an alphameric field describing the problem input

III. ioptdc, ioptst, CfACRR, Vbed, bedeps, ioptR, ioptT

A. ioptdc = flag for decay chain calculations. 0:read input and do calc. 1:read input, no calc.

B. ioptst = flag for stress-strain calculations. 0:read input and do calc. 1:read input, no calc.

C. CfACRR = coupling factor to convert input power (W) to actual power in the fuel (W/m^3-bed).

D. Vbed = Bed volume (m^3). The total fission source used in the code is calculated as Q*CfACRR*Vbed/29e-12.

E. ioptR = Release coefficient option.
= 0: Read in release coefficients in a table.
= 1: Calculate from the temperature-time table and diffusion and geometry data.

F. ioptT = Temperature option.
= 0: Read in temperature-time table and use as uniform temperature.
= 1: Calculate a steady-state temperature profile from the power-time table, material and property data, and heat transfer

coefficient, with the temperature-time table as a boundary condition.

= 2: Read in temperature-time table, read in spatial temperature distribution table and Q (activation energy) table to adjust diffusional release coefficients.

IV. tstop, tunits, dtprint, pincr

A. tstop = problem end time in units of days or seconds (see tunits variable).

B. tunits = time units for tstop, one of: 'd' = days, 'h'= hours, 'm'= minutes, or 's' = seconds.

C. dtprint = initial output time interval (s). Both dtprint and the internal timestep are increased by pincr every dtprint seconds.

D. pincr = factor to increase timestep and dtprint by every dtprint seconds (1.1).

V. Npow/qtim,Qtab (Power-time table, Npow pairs of points, 1 pair/line).

A. Npow = number of points in the time-power table.

B. qtim = time point (s).

C. Qtab = input power at time qtim (W reactor).

NOTE: Qtab is used as the output time controller, so that an output occurs at every Qtab entry time.

VI. nhtab/htim, htctab (heat transfer coefficient-time table (W/m^2K).

A. nhtab = number of points in the time-heat transfer coefficient table.

B. htim = time point (s).

C. htctab = heat transfer coefficient (W/m^2K).

VII. nttab/ttim, tctab (coolant temperature-time table)

A. nttab = number of points in the time-coolant temperature table.

B. ttim = time point (s).

C. tctab = coolant temperature (K). This is used as a boundary temperature if the temperature calculation is on (see ioptT) or the uniform particle temperature if the calculation is off.

VIII. ndt/dtt, dtmax (dtmax-time table)

A. ndt = number of points in the time-dtmax table.

B. dtt = time point (s).

C. dtmax = maximum timestep at time dtt (s). Timesteps are interpolated between points in the table. If the run time exceeds the last time in the table, the last dtmax value is kept. This behavior is true for all tables in the input.

IX. Vratio, Vfrac, atom_limit

A. Vratio = ratio of total particle volume to volume of 1 particle = number of particles. This is used only in the calculation of release coefficients from diffusion coefficients (see ioptR).

B. Vfrac = fraction of released fission products sampled, used to multiply output activities. Vfrac can also be used to convert the output activities (counts/s) to other units, ie, Curies (2.703e-11), or to correct for detector efficiency.

C. atom_limit = number of atoms below which the nuclide is dropped from the decay calculations, if power is zero (1e4).

X. nact (nach(i), nanu(i), i=1,nact)

A. nact = number of activities to monitor and output on tty.

B. nach = decay chain for ith monitored activity.

C. nanu = nuclide in decay chain nach for ith monitored activity.

XI. nchain, decaymin, decaymax

A. nchain = number of decay chains in problem.

B. decaymin = Minimum decay constant allowed while extracting nuclides from database (2×10^{-8}, or a halflife of ~1yr).

C. decaymax = Maximum decay constant allowed while extracting nuclides from database (0.1, or a halflife of ~7sec).

XII. nlayers/matid, del, MW, rho, Cp, k, rad

A. nlayers = number of layers in particle. The next line is repeated for each layer.

B. matid = material id label for layer n.

C. del = thickness of layer n (m).

D. MW = molecular weight of material (kg/kmol).

E. rho = density (kg/m^3).

F. Cp = sepcific heat capacity (J/kg-K).

G. k = thermal conductivity (W/m-K).

H. rad = outer radius of layer n (m).

The following sections (XIII-XVIII) are repeated nchain times to describe the decay chains.

XIII. labdc

A. labdc = alphameric label for decay chain. If the 1st 2 characters are not "rd", ie, dc88, then the decay chain parameters are read from input. Otherwise, the parameters are read from the decay chain database and lines XVI and XVII are read instead of XIV and XV.

XIV. nnuc

A. nnuc = number of nuclides in decay chain.

The following section is repeated nnuc times.

XV. labnuc/dfy, decay, fZ1toZ, fZ1MtoZ, fZMtoZ, irel

A. labnuc = nuclide label ,ie, Br88.

B. dfy = direct fission yield fraction.

C. decay = decay constant (1/s).

D. fZ1toZ = branching fraction, parent ground state (Z-1) to daughter (Z).

E. fZ1MtoZ = branching fraction, parent metastable state (Z-1M) to daughter (Z).

F. fZMtoZ = branching fraction, daughter metastable (ZM) to daughter (Z). Note that if the current daughter nuclide is metastable, it is considered "Z" for purposes of entering the branching fractions, although the fZMtoZ will always be 0.

G. irel = release coefficient index for release (atomic number Z or 0 for no release). No release of a specific type will occur if the corresponding entry does not exist in the release table.

XVI. Nucstart, Nucend, Nnucin (Read if decay chain label started with "rd").

A. Nucstart = number of starting nuclide from start of record in database. If 0, this will default to 1.

B. Nucend = number of ending nuclide in record. If 0, this defaults to number in database record.

C. Nnucin = number of nuclides to use in record. This is used in conjunction with Nucstart and will override Nucend if > 0.

XVII. (irel(n), n=1,Nnucin) (Read if decay chain label started with "rd").

A. irel = release coefficient index for release (atomic number Z or 0 for no release). No release of a specific type will occur if the corresponding entry does not exist in the release table.

XVIII. Gamma energy intensities of measured species (1-nnuc)

A. gami = gamma energy intensity for nuclide, used to correct for measurements. There are nnuc of these on a line.

XIX. Ndiff

A. Ndiff = number of families of diffusion coefficient equations. There are Ndiff rows of parameters entered.

XX. (NZ, D12, Qdiff, n=1,nlayers) diffusion parameters for each layer, 1 family/line.

A. NZ = nuclide atomic number.

B. D12 = lead coefficient in diffusion equation for material in layer n (m^2/s).

C. Qdiff = activation energy for material in layer n (J/mol/K).

XXI. Nrrate(i), i = 1, 3

A. Nrrate = number of families (rows) in time-release coefficient tables. There will be one row for each type of nuclide generally. There are 3 tables: (1) Diffusional, (2) Direct (proportional to parent nuclide), and (3) Surface (proportional to nuclide).

XXII. ntl/(trell, n=1,ntl)

A. ntl = number of time points in table.

B. trell = time point (s), repeated ntl times, max 8 times per line.

XXIII. NZ, (rell, n=1,ntl)

A. NZ = Index for release family (atomic number Z).

B. rell = Diffusional release coefficient, 1 value for each time trell (1/s), 8 values per line. If there are more than 8 entries for release family Z, the succeeding lines contain up to 8 values for rell each without the leading NZ. There are nrell families of coefficients.

XXIV. nt2/(trel2, n=1,nt2)

A. nt2 = number of time points in table.

B. trel2 = time point (s), repeated nt2 times, max 8 times per line.

XXV. NZ, (rel2, n=1,nt2)

A. NZ = Index for release family (atomic number Z).

B. rel2 = Direct release coefficient, 1 value for each time trel2 (1/s), 8 values per line. If there are more than 8 entries for release family Z, the succeeding lines contain up to 8 values for rel2 each without the leading NZ. There are nrel2 rows of coefficients.

XXVI. nt3/(trel3, n=1,nt3)

A. nt3 = number of time points in table.

B. trel3 = time point (s), repeated nt3 times, max 8 times per line.

XXVII. NZ, (rel3, n=1,nt3)

A. NZ = Index for release family (atomic number Z).

B. rel3 = Surface release coefficient, 1 value for each time trel3 (1/s), 8 values per line. If there are more than 8 entries for release family Z, the succeeding lines contain up to 8 values for rel3 each without the leading NZ. There are nrel3 rows of coefficients.

The difference between diffusional, direct, and surface release coefficients is that "diffusional" release coefficients multiply the number of atoms of the nuclide in the decay equations and are intended to represent release through intact coatings, although they could also be used instead of a separate surface release table; the "direct" release coefficients multiply the decays per second of the parent nuclides. The "surface" table also multiplies the number of atoms of the nuclide, but is unaffected by the temperature shape table, if used. There is no other implication about the actual transport mechanisms involved except that two (tables 1and 3) are proportional to the number of atoms of the nuclide and the other (table 2) is proportional to the decay rate of the parent(s).

The following lines are only read if the shape table option (ioptT = 2) is used.

XXVIII. irm, jzm, drt, dzt, rin, Tfact, inorm

- A. irm = number of radial nodes in the shape table (bed).
- B. jzm = number of axial nodes in the shape table (bed).
- C. drt = Width of each radial node in the bed (m).
- D. dzt = Height of each axial node in the bed (m).
- E. rin = Inner radius of bed (m).
- F. Tfact = Temperature factor used to normalize bed if inorm = 0. This would usually correspond to the temperature assumed in calculating release coefficients, so that release coefficients for positions in the bed with this temperature would be unaffected by the correction factors in the shape table. (K)
- G. inorm
  - = Normalization option flag.
  - = 0: Usual option, use Tfact as normalization temperature.
  - = 1: Use peak temperature in shape table (bed temperatures) as normalization.
  - = 2: Use volume-averaged temperature (calculated internally) as normalization.

The bed temperature shape table, irm values per row, jzm rows, is read from the file **temp.shp**. Also necessary is a table of effective activation energies Qa (for the coating, if that is controlling release) (kJ/mol-K) and atomic number nZ. These are read from file **qzdif.dat**, which has records with 2 values per line of the form nZ, Qa. If the atomic number for a nuclide is not present in this file but a release coefficient is used, a warning is printed at the beginning of the calculation and the temperature adjustment is skipped for that nuclide.

XXIX. nreg

- A. nreg = Number of regions

XXX. (nel(i), i=1,nreg)

- A. nel = Number of elements per region

XXXI. rad(i), i=1,nreg

A. rad = Inner radius of region i (m). There are nreg of these radii, one per line.

XXXII. rad(nreg+1)

A. rad(nreg+1) = Outer radius of region nreg (m).

XXXIII. (trefr(i), i=1,nreg)

A. trefr = Thermal expansion reference temperature for region i (K).

XXXIV. icreep, nci

A. icreep = creep flag (0:off, 1:on)

B. nci = number of creep iterations (2).

XXXV. iplastic, npi

A. iplastic = plastic flag (0:off, 1:on) **(NOTE: THIS OPTION DOES NOT WORK IN HEISHI V. 2.0-2.1)**

B. npi = number of plastic iterations (3).

XXXVI. igrain

A. igrain = grain growth flag (0:off, 1:on)

XXXVII. iffrac

A. iffrac = failure fraction flag (0:off, 1:on)

XXXVIII. (imat(i), i=1,nreg)

A. imat = material id numbers, used to select correct internal material property function for each region.

XXXIX. (Qfac(i), i=1,nreg)

A. Qfac = Power factor for region i. This factor multiplies CfACRR*Q.

XL. gr0(i), gQ(i), Akg(i), i=1,nreg, nreg lines

A. gr0 = original grain size for region i (m).

B. gQ = Activation energy for grain growth for region i (J/mol).

C. Akg = grain growth constant ($m^2/s^{1/2}$).

XLI. fm, sf0

A. fm = Weibull modulus in failure fraction model

B. sf0 = original failure stress in Weibull model (Pa).

XLII. timestep

A. timestep = timestep for stress-strain module (s)

XLIII. prntint

A. prntint = print interval for stress-strain module (s).

XLIV. ihtflag, nthi, gam

A. ihtflag = heat transfer flag (0:off, 1:on). This controls whether the temperature solution routines are used (on) or the coolant temperature is used (off).

B. nthi = number of heat transfer iterations (2)

C. gam = fractional implicitness used in heat transfer solution (0:explicit, 0.5:Crank-Nicholson, 1:implicit).

XLV. ibcht, ibcstr

A. ibcht = heat transfer inner boundary condition flag (0:flux, 1:zero gradient).

B. ibcstr = stress-strain inner boundary condition flag (0:pressure, 1:zero displacement).

XLVI. npresi/tt1(i),presit(i)

A. npresi = number of time-pressure pairs in inner pressure-time table

B. tt1 = time point (s).

C. presit = inner boundary pressure (Pa).

XLVII. npreso/tt2(i),presot(i)

A. npreso = number of time-pressure pairs in outer pressure-time table

B. tt2 = time point (s).

C. presot = outer boundary pressure (Pa).

XLVIII. nhflux/tt4(i),hfluxt(i)

A. nhflux = number of time-heat flux pairs in inner heatflux-time table.

B. tt4 = time point (s).

C. hfluxt = inner boundary heat flux (W/m^2).

OUTPUT FILES

hs2.out

This is a people-readable short output edit containing (1) a header with the HEISHI version number and run date; (2) total number of fissions, the result of integrating the power history multiplied by CfACRR and Vbed from time 0 to tstop; (3) decay chain data as read from either **hs2.in** or **fpdb.asc**; (4) edit of stress-strain module input; (5) stress-strain output edits.

labs.dat

This file contains the nuclide labels for each decay chain. The file is used by the dcred

postprocessing program. The records contain

labdc(nc), (labnuc(n,nc), n=1,nnuch(nc))

where
nc = decay chain index
labdc(nc) = decay chain label
labnuc(n,nc) = label for nuclide n of decay chain nc
nnuch(nc) = number of nuclides used in decay chain nc.

There is one set of these records for each decay chain, nchain total. The output format = (1x,a8/1x,10(a8,2x)).

The following data files all have the same format: **dca.dat, dcn.dat, dcna.dat, dcr.dat, dcrn.dat, dcre.dat.**

dca.dat

This contains chain and activity data for released nuclides. The initial record is

nchain
(nnuch(n),n=1,nchain)

where
nchain = number of decay chains
nnuch(n) = number of nuclides used in decay chain n.
format = (i6/20i6)

+--repeat following records for each output time---

+--repeat for each chain nc---
t,td,dca(n),n=1,nnuch(nc))
---end repeat for nc---

---end repeat for time t---

where
t = output time (s)
td = output time (days),
dca(n) = activity for released nuclide n in chain nc (calculated as decay*xnr*Vfrac*ge).
format = (10(1pe12.5))

dcn.dat contains number of atoms of retained nuclides.

dcna.dat contains the activity of atoms of retained nuclides calculated as decay*xn*ge.

dcr.dat contains release-to-birth ratios of released nuclides calculated as xn2/(Fissions*dfy), where
Fissions = total number of fissions
dfy = direct fission yield of nuclide.

dcrn.dat contains the number of atoms of released nuclides.

dcre.dat contains release coefficients for the nuclides (this is usually only of interest if the ioptT = 2 option was selected).

The following files are contain output from the stress-strain module.

pstress.dat

Miscellaneous data from the stress-strain module. The main difference between this and the **pstress.plt** file is that initial values of mechanical properties are included.

pstress.plt

Output at each stress-strain output time, contains stress-strain data from the stress-strain module. Values are output for each finite difference node at each output time.

+--repeat following records for each output time---
+--repeat for each radial node---

t,rad,d,sh,sr,eh,er,epphc,epphp,|sh-sr|,yield,temp

---end repeat over radial nodes---
---end repeat for each time---

where
t = stress-strain output time (s)
rad = radial position (m)
d = radial displacement (m)
sh = hoop stress (Pa)
sr = radial stress (Pa)
eh = hoop strain
er = radial strain
epphc = hoop creep strain
epphp = hoop plastic strain
|sh-sr| = shear stress (Pa)

yield = yield stress (Pa)
temp = temperature (K).

format = (1x,12(1pe10.3,1x))

hsgeom.dat

Output at each stress-strain output time, contains data from the grain growth and failure fraction routines.

+--repeat following record for each output time---

t,ff,sf,(gr(j),treg(j),j=1,nreg)

---end repeat for each time---

where
t = stress-strain output time (s)
ff = failure fraction
sf = Weibull failure stress (Pa)
gr(j) = grain size for material region j
treg(j) = average temperature for region j
nreg = number of regions (layers).

format = (1x,12(1pe10.3,1x))

Distribution

John Metzger
Grumman Aerospace
M/S B09-25
Bethpage, NY 11714

Phillips Laboratory/VT-X (2)
attn: Gerry Gibson
Charles Harmon
3550 Aberdeen Ave SE
Kirtland AFB, NM 87117-5776

Brookhaven National Laboratory (2)
attn: Bob Barletta
Don Sweitzer
Building 701
Upton, L. I. NY 11973

Helen Moeller
Babcock & Wilcox
Mt. Athos Rd Rt. 726 POB 11165
Lynchburg, VA 24506-1165

Babcock & Wilcox (3)
attn: DeWayne Husser
Jack Kerr
Matt Ales
Mt. Athos Rd Rt. 726 POB 785
Lynchburg, VA 24506-0785

Walter Stark
Los Alamos National Laboratory
POB 1663 MS E505
Los Alamos, NM 87545

Knolls Atomic Power Laboratory (2)
attn: J. A. Robillard
G. A. Newsome
POB 1072 Bldg 62
Schenectady, NY 12301-1072

MS 0835 R. E. Hogan (1513)
MS 0340 R. J. Bourcier (1832)
MS 0736 N. R. Ortiz (6400)
MS 1176 A. C. Marshall (6474)
MS 1143 J. K. Rice (6500)
MS 1144 J. V. Walker (6501)
MS 0835 D. Dobranich (1513)
MS 1175 G. S. Rightley (6513)
MS 1145 S. C. Bourcier (6514)
MS 1145 R. L. Coats (6514)
MS 1145 E. J. Parma (6514)
MS 1145 P. S. Pickard (6514)
MS 1145 A. J. Suo-Anttila (6514)
MS 1145 D. G. Talley (6514)
MS 1145 S. A. Wright (6514)
MS 1151 M. Berman (4701)
MS 0744 M. J. Rightley (6403)
MS 1175 M. F. Young (6513) (20)
MS 0756 G. C. Allen (6607)
MS 0899 Technical Library (7141) (5)
MS 0619 Technical Publications (7151)
MS 0100 Document Processing for DOE/OSTI (7613) (10)
MS 9018 Central Technical Files (8523)